Volume averaging based integration method in the context of XFEM-cohesive zone model coupling

Konstantinos Nikolakopoulos, Jean-Philippe Crété, Patrice Longère

Volume averaging based integration method in the context of XFEM-cohesive zone model coupling

Konstantinos Nikolakopoulos[a,b], Jean-Philippe Crete[b,*], Patrice Longere[a]

[a] ISAE-SUPAERO, ICA, Université de Toulouse, Toulouse, France
[b] Laboratoire Quartz, SUPMECA, Saint-Ouen, France

A B S T R A C T

The main issue of the extended finite element method (XFEM) is the numerical integration of the system of equilibrium equations. Indeed, in order to have a correct displacement jump vector, the integration needs to be achieved on both sides of the discontinuity and thus requires the existence of integration points on both sides of the discontinuity. A volume averaging based integration method is developed in the present work alleviating this constraint and applied to XFEM coupled with cohesive zone model in a three-dimensional formulation. Moreover, unlike other widely used integration methods, the proposed method does not require the a priori knowledge of the position of the discontinuity inside the finite element nor the projection of the state variables.

Keywords:
X-FEM
Cohesive zone model
Numerical integration
Volume averaging scheme
Incompressibility

1. Introduction

The main issue of the extended finite element method (XFEM) is the numerical integration of the system of equilibrium equations, in particular when XFEM is coupled with a cohesive zone model (CZM). Indeed, CZM is generally governed by a relationship between the displacement jump vector across the discontinuity and the cohesive traction forces that prevent the crack from opening. If there is no integration point on one of the two sides of the crack, classic Gauss quadrature does not provide an accurate enough integration leading to wrong calculations of the stiffness matrix, the internal forces and then the displacement jump vector. In literature there exist several approaches aiming at palliating this deficiency.

The most commonly used technique is the subdivision of elements, with examples in [1–3], wherein the element sub-volumes V^+ and V^-, separated by the crack, are triangulated into subdomains, viz. triangles (if $\boldsymbol{R}^2$) or tetrahedra (if $\boldsymbol{R}^3$), each containing one or more Gauss points. The standard Gauss quadrature is then applied for the integration of the weak form in every subdomain. This method should not be confused with the mesh modification techniques, see [4], as the said partitioning is realized only for the integration and thus does not introduce any supplementary degrees of freedom. The element subdivision based technique is well adapted for elastic materials or for structures with initial defects. It implies the projection of state variables on the new integration points. This procedure can be both computationally cumbersome and leads to errors, especially in the case of elasto-plastic materials whose response is path-dependent.

To address the aforementioned issue, Elguedj et al. [5] instead proposed to raise significantly the number of Gauss points (64 in 2D), as a means to ensure that there is always at least one integration point on both sides of the discontinuity (if the discontinuity crosses the element near a node, the discontinuity is slightly shifted without substantial modification of the discontinuity path). With this technique, there is no projection requirement but the extension in 3D requires 512 integration points, increasing drastically the cost and the time of calculation.

Martin et al. [6] proposed the substitution of the discontinuous Heaviside function, in the elements cut by the discontinuity, by a new continuous enrichment function. Using this technique, there is no issue of projection of the state variables and no modification of the crack path, for a number of Gauss point of 27 for a linear hexahedron, which also leads to an increase in the computation time. Moreover, the authors do not discuss the use of the B-Bar approach (see [7]) to prevent volumetric locking in the case of a strongly nonlinear behavior material.

The volume averaging based integration method developed in the present work is inspired from the approach developed in Belytschko [8]. The method allows for alleviating the need for the existence of integration points on both sides of the discontinuity and is applied to XFEM coupled with cohesive zone model in a

* Corresponding author.
E-mail address: jean-philippe.crete@supmeca.fr (J.-P. Crete).

https://doi.org/10.1016/j.mechrescom.2020.103485

three-dimensional formulation. Moreover, unlike other widely used integration methods, the proposed method does not require the a priori knowledge of the position of the discontinuity inside the finite element nor the projection of the state variables.

In Section 2 the formulation of the X-FEM and the coupling with a cohesive zone model are recalled. The numerical integration of the equilibrium equations, including the B-Bar approach, is detailed in Section 3. Two applications, viz. with and without initial discontinuity, are presented in Section 4, in view of comparing the proposed technique with classical approaches. Concluding remarks are given in Section 5.

2. X-FEM – CZM coupling

The eXtended Finite Element Method [1,9] has become one of the most widely used methods for the simulation of crack propagation in engineering structures. It is based on the idea of embedding the crack within the finite element. The kinematics of the crack is accounted for by enriching the regular displacement field of the finite element with additional degrees of freedom. One of its most important advantages is that the crack can propagate independently of the meshing, without the need for the a priori knowledge of the crack path. XFEM has demonstrated its performances for brittle and quasi-brittle materials, see [3,10]. Now, in the case of strongly non-linear elastoplastic materials subject to ductile damage, this method may lead to unrealistic results, see [11]. Indeed, the activation of the enriched dofs in an element leads to a sudden (traction free) crack opening. Yet, in these materials, the failure should be gradual. To tackle this problem, the concept of combining XFEM with a cohesive segment [2] is adopted in the present work.

2.1. X-FEM formulation

In this work, the "shifted basis" formulation of the X-FEM [12] without singular functions is used. The discretized total displacement field u(x) accordingly reads

$$u(x) = \sum_n N_i a_i + \sum_m \big(H(x) - H_j\big) N_j b_j \tag{1.1}$$

where Ni is the ith standard FE shape function, n the number of nodes, a_i the ith standard displacement degree of freedom, m the number of enriched nodes and b_j the jth additional degree of freedom associated to the jth node. H is the Heaviside function, which equals to $+0.5$ if a point is located at the "positive" side of the discontinuity and -0.5 else and H_j the value of the Heaviside function at each node.

The coupling between XFEM and CZM [13] consists in inserting a cohesive segment in the strong discontinuity in order to form a "cohesive strong discontinuity". The XFEM formulation is adopted and the system to be solved reduces to the following linear form:

$$[K]\begin{Bmatrix} da \\ db \end{Bmatrix} = -\begin{Bmatrix} \int_{V^e} \boldsymbol{B}^T \boldsymbol{\sigma} dV \\ \int_{V^e} \boldsymbol{B^*}^T \boldsymbol{\sigma} dV + \int_{\Gamma_D} \boldsymbol{N}^T \boldsymbol{T}_{loc} d\Gamma \end{Bmatrix}, \tag{1.2}$$

where

$$[K] = \begin{bmatrix} \int_{V^e} \boldsymbol{B}^T \boldsymbol{D^t} \boldsymbol{B} dV & \int_{V^e} \boldsymbol{B}^T \boldsymbol{D^t} \boldsymbol{B^*} dV \\ \int_{V^e} \boldsymbol{B^*}^T \boldsymbol{D^t} \boldsymbol{B} dV & \int_{V^e} \boldsymbol{B^*}^T \boldsymbol{D^t} \boldsymbol{B^*} dV + 4 \int_{\Gamma_D} \boldsymbol{N}^T \boldsymbol{C}_{loc} \boldsymbol{N} d\Gamma \end{bmatrix} \tag{1.3}$$

Where $\boldsymbol{\sigma}$ is the stress vector, $\boldsymbol{D^t}$ the elastic-plastic tangent operator, $\boldsymbol{T}_{loc}$ the cohesive tractions vector, $\boldsymbol{C}_{loc}$ the cohesive stiffness matrix, $\boldsymbol{B}$ the spatial derivatives matrix of the shape functions, $\boldsymbol{B^*}$ the spatial derivatives matrix of the $(H(x) - H_j)N_j$ functions and Γ_D the discontinuity. The subscript *loc* refers to the local frame of the localization band.

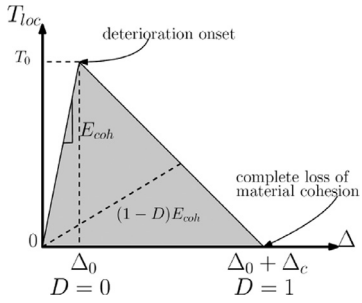

Fig. 1. Bi-linear cohesive law.

2.2. Adopted CZM approaches

As can be seen in Eqs. (1.2) and (1.3), the coupling of CZM with the XFEM implies the incorporation of the cohesive tractions vector $\boldsymbol{T}_{loc}$ and the cohesive stiffness matrix $\boldsymbol{C}_{loc}$, in the finite element formulation. The method of calculation of the above physical quantities, via the traction separation law (TSL), strongly depends on the material and engineering application under consideration [14]. In the present work, two different applications are considered (Sections 4.1 and 4.2), leading to the use of two different cohesive laws (Sections 2.2.1 and 2.2.2).

Both laws are activated as soon as the deterioration criterion is met. Their common basis is inspired from the approach in Camanho [15] where the evolution of the softening branch of the cohesive law is governed by a de-cohesion variable $D \in [0,1]$, where 0 denotes a healthy element and 1 a fully damaged element. The argument Δ of the function $D = f(\Delta)$ is an equivalent displacement that takes into account the displacement jump vector $\underline{\boldsymbol{\delta}}$, with δ_1 the normal component and $\delta_{2,3}$ the shear components (expressed in the local frame of the localization band):

$$\Delta = \sqrt{\langle\langle\delta_1\rangle\rangle^2 + \delta_2^2 + \delta_3^2}, \text{ where } \langle\langle\delta_1\rangle\rangle = \max(0, \delta_1) \tag{1.4}$$

For the sake of simplicity, contact is not treated here.

The evolution law of the de-cohesion variable is assumed herein of the form

$$D = \begin{cases} 0, & if\ \Delta \le \Delta_0 \\ \frac{\Delta - \Delta_0}{\Delta_c}, & if\ \Delta_0 < \Delta < \Delta_0 + \Delta_c \\ 1, & if\ else \end{cases} \tag{1.5}$$

Δ_0 is the equivalent displacement at the degradation occurrence and $\Delta_0+\Delta_c$ the critical value of the equivalent displacement at the complete fracture of the element.

2.2.1. Pre-existing discontinuity in the structure

Adhesively joined assemblies and laminate composites contain pre-existing discontinuities. The numerical analysis of such bonded structures at the meso–scale is generally conducted by means of cohesive interfaces/elements whose behavior obeys a TSL generally characterized by a linear ascending branch, possibly a plateau, and then a linear or nonlinear softening branch. Depending on the authors, the criteria for the loss of (initial) linearity (deterioration onset) and ultimate failure (complete de-cohesion) are expressed mostly as a combination of two material parameters, e.g. in terms of critical displacement and critical traction force [16] or critical traction force and energy release rate [17]. For simplicity, we are here considering a bi-linear cohesive law as depicted in Fig. 1. This cohesive law will be used later in Section 4.1.

The cohesive tractions vector corresponding to Fig. 1 is expressed as:

$$\underline{T}_{loc} = [C_{loc}] \times \underline{\delta} \tag{1.6}$$

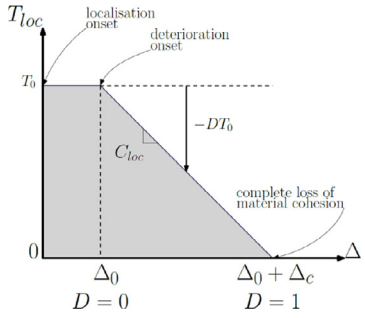

Fig. 2. Linear/plateau cohesive law.

with

$$C_{loc}(i,j) = (1-D)P_k(i,j) \tag{1.7}$$

where $P_k(i,i) = E_{coh}$, the value of the cohesive law slope. The other components of the matrix are zero, leading to a non-coupling of the normal and shear effects.

The deterioration and complete failure onsets are here defined by critical displacements. The cohesive law accordingly requires three independent constant quantities, viz. E_{coh}, Δ_0, Δ_c.

2.2.2. No pre-existing discontinuity in the structure

In continuous bodies initially exempt of defects, the crack formation is generally preceded by a strain/damage localization possibly induced by microvoid/microcrack coalescence. The progressive deterioration of the mechanical properties of the localization band containing material may be described via a cohesive law. In this case the elastic response is the one of the bulk material [18], and the cohesive law possesses only a plateau and a softening branch. Once again, criteria are needed to trigger the cohesive law and ultimate fracture. A particular attention must be paid to ensure the stress continuity at the cohesive law onset. For example, the initial (maximum) traction can be a fixed value or a value that is determined in the element at the onset as a function of the current stress state.

In Fig. 2 is depicted an example of a plateau/linear softening cohesive law; as used in this work in the case of no pre-existing discontinuity in Section 4.2.

The initial traction at localization occurrence in the element is calculated through the use of a stress tensor $\underline{\underline{\tilde{\sigma}}}$ averaged over all Gauss points of the element as follows

$$\underline{T}_0 = \left\langle \underline{\underline{\tilde{\sigma}}}\,\underline{n} \right\rangle_{loc} \tag{1.8}$$

$\underline{T}_0$ is thus not a constant quantity and is different for each element since it results from its current stress state at the moment of localization. It may also be defined arbitrarily or result from a bifurcation analysis.

The cohesive tractions vector is expressed as:

$$\underline{T}_{\text{loc}} = (1-D)\underline{T}_0 \tag{1.9}$$

The tangent matrix of the cohesive law in the softening regime is obtained by

$$C_{loc}(i,j) = \frac{\partial T_{loc}(i)}{\partial \delta_j} = -\frac{\partial D}{\partial \delta_j} T_0(i) = -\frac{1}{\Delta_c}\frac{\delta_j}{\Delta} T_0(i) \tag{1.10}$$

with $C_{loc}(i,1) = 0$ if $\delta_1 < 0$

The cohesive law accordingly requires two independent constant quantities, viz. Δ_0, Δ_c.

As soon as the critical value of the de-cohesion variable D is reached the cohesive tractions are automatically set to zero, leading to a traction free crack. The value D_c at failure can thus be lower than 1 depending on the material behavior. In the present work it is taken equal to 0.5.

3. Numerical integration

In the following are outlined the three integration techniques considered in the present work.

3.1. Standard Gauss integration

It is reminded that the discrete standard Gauss integration consists in computing

$$I = \sum_{i=1}^{nint} f\left(\mathrm{H}\left(\underline{\xi}_i\right), \underline{\xi}_i, \ldots\right) w_i J\left(\underline{\xi}_i\right) \tag{1.11}$$

where I can be the stiffness matrix or the internal forces vector, *nint* the number of Gauss points, $\underline{\xi}_i$ the vector containing the local coordinates of the Gauss point, w_i the weight of the Gauss point, J the determinant of the Jacobian and f a function of the position of the integration point with respect to the discontinuity.

3.2. Sub-division technique

As was stated in Section 1 the subdivision of hexahedral elements into tetrahedra is the most widely used technique for the numerical integration of elements crossed by discontinuities. After the subdivision, the field variables are projected from the current integration points onto new ones belonging to the tetrahedra, and then a standard Gauss integration rule is applied on each sub-element.

3.3. Volume averaging integration (VAI)

The volume of the element crossed by the discontinuity is split into two sub-volumes V^+*and* V^- separated by the discontinuity, see Fig. 3 left. The proposed volume averaging integration method makes use of a modified quadrature rule that performs the integration twice over the standard Gauss points of the element by means of an averaging of the contributions of the two sub-volumes $V^+$and V^-:

$$I = \frac{V^-}{V^e}\sum_{i=1}^{nint} f\left(-0.5, \underline{\xi}_i, \ldots\right) w_i J\left(\underline{\xi}_i\right) + \frac{V^+}{V^e}\sum_{i=1}^{nint} f\left(+0.5, \underline{\xi}_i, \ldots\right) w_i J\left(\underline{\xi}_i\right) \tag{1.12}$$

According to (1.12), the contribution of a given sub-volume to I consists in a sum over all integration points of the element while assigning the value $+0.5$ (V^+) or -0.5 (V^-) to H in (1.11) and weighting the result by the ratio of the sub-volume over the total volume of the element. VAI principle is depicted in the visual representation of a cut element with 8 integration points (red marks) in Fig. 3.

It is noteworthy that this method has been originally proposed by Belytschko [8] and has been very recently applied by Jin et al. [19] within an embedded-band based approach. The authors do not, however, address the case where the band crosses the element in such a way that one sub-volume does not contain any integration points, a case that will be precisely addressed in the present work. The VAI technique is applied here in a different context, i.e. to XFEM coupled with a cohesive strong discontinuity and compared to other integration methods.

The proposed scheme must be completed by the use of the B-Bar approach in order to deal with incompressibility. Indeed, in order to alleviate volumetric locking in nearly-incompressible media the B-bar approach is employed (see Hughes [7]). The matrix B

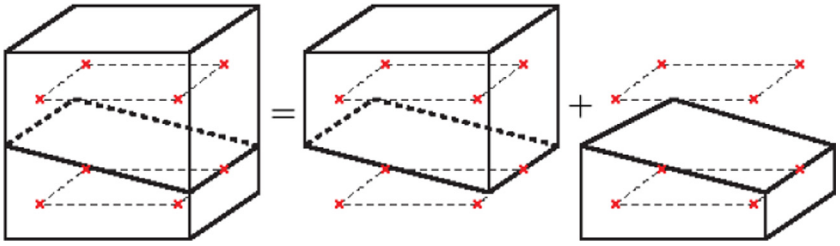

Fig. 3. Visual representation of the "volume averaging" integration scheme.

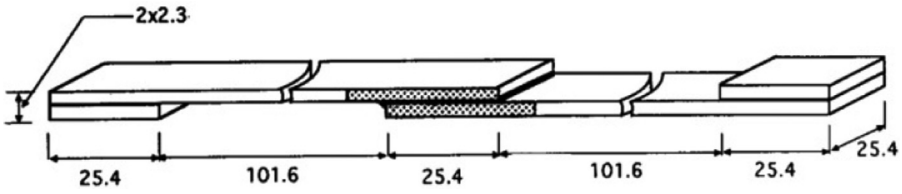

Fig. 4. Single lap specimen dimensions [22].

containing the spatial derivatives of the shape functions can be decomposed into a deviatoric and a dilatational component, i.e. B_{dev} and B_{dil} respectively:

$$B = \begin{bmatrix} B_{dil} \\ --- \\ B_{dev} \end{bmatrix} \tag{1.13}$$

The dilatational part is responsible for an over-stiff response. To palliate this deficiency, the component B_{dil} in (1.13) is replaced by a new $\bar{B}_{dil}$ component in a way that volume growth is each integration point is replaced by a value averaged over all points:

$$\bar{B} = \begin{bmatrix} \bar{B}_{dil} \\ \hline B_{dev} \end{bmatrix} \Rightarrow \tag{1.14}$$

$$\bar{B}_i = \begin{bmatrix} N_{i,x} + \tilde{\tilde{N}}_{i,x} & \tilde{\tilde{N}}_{i,y} & \tilde{\tilde{N}}_{i,z} \\ \tilde{\tilde{N}}_{i,x} & N_{i,y} + \tilde{\tilde{N}}_{i,y} & \tilde{\tilde{N}}_{i,z} \\ \tilde{\tilde{N}}_{i,x} & \tilde{\tilde{N}}_{i,y} & N_{i,z} + \tilde{\tilde{N}}_{i,z} \\ N_{i,y} & N_{i,x} & 0 \\ N_{i,z} & 0 & N_{i,x} \\ 0 & N_{i,z} & N_{i,y} \end{bmatrix} \tag{1.15}$$

where

$$\tilde{\tilde{N}}_{i,x} = \frac{1}{3}(\langle N_{i,x} \rangle - N_{i,x}) \tag{1.16}$$

$\langle N_{i,x} \rangle$ is the averaged value of $N_{i,x}$ over all integration points.

For the enriched nodes, the B-bar matrix takes the form $\bar{B}_i^* = (H(x) - H_i)\bar{B}_i$. For more details about the implementation of the B-bar approach in the framework of ABAQUS the reader can refer to Shi et al. [20].

4. Application

The methodology coupling XFEM and CZM outlined in Section 2.1 has been implemented as a user element subroutine (UEL) in the commercial finite element computation code ABAQUS. In order to verify the ability of VAI to perform an accurate integration in the case of embedded cohesive strong discontinuities, two different applications are taken into consideration: (i) the single lap adhesive joint in Fig. 4 and (ii) the tensile specimen in Fig. 7.

In both numerical tests the infinitesimal strain theory is assumed and the tetrahedral elements created during the subdivision stage have one integration point. As shown in 2D in Seabra et al. [21], by choosing a single point integration rule, more incompressible modes are reproducible, which can alleviate volumetric locking.

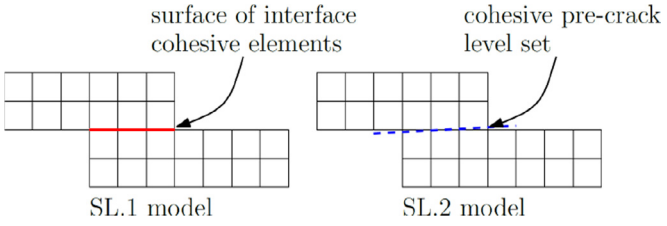

Fig. 5. Visualization of the two different single lap models.

In the sequel, the developed 'volume averaging integration' or VAI technique described in Section 3.2 is notably assessed with respect to the subdivision technique above.

4.1. Single lap joint test – Pre-existing discontinuity

The single lap specimen, see Fig. 4, used in this work was taken from Tsai [22]. Two different finite element models were created, see Fig. 5. The first model, designated SL.1, contained an explicitly given surface of zero-thickness ABAQUS cohesive elements between the adherents, see Fig. 5 left.

For the second model, designated SL.2, the discontinuity was introduced as the level-set of a cohesive pre-crack crossing the elements in a way that one of the created sub-volumes does not contain any integration points, see Fig. 5 right. This choice is made in order to verify the accuracy of the proposed scheme in the most extreme conditions.

Both models were discretized using a structured three-dimensional meshing of full integration hexahedral elements (C3D8 ABAQUS elements) of 1 mm length, therefore for "SL.1″ the length of each cohesive element is also of 1 mm.

The material considered for the adherents is a rate and temperature independent mild steel with $E = 210$ GPa and $\nu = 0.33$. The plastic flow condition is defined via the Von Mises yield criterion:

$$f(\underline{\underline{\sigma}}, \sigma_Y) = \sigma_{eq} - \sigma_Y = 0 \tag{1.17}$$

where $\underline{\underline{\sigma}}$ is the Cauchy stress tensor and σ_{eq} the equivalent stress defined by

$$\sigma_{eq} = \sqrt{\frac{3}{2}\underline{\underline{s}} : \underline{\underline{s}}; \underline{\underline{s}} = \underline{\underline{\sigma}} - \frac{1}{3}Tr\underline{\underline{\sigma}}\ \underline{\underline{I}}} \tag{1.18}$$

Table 1
Hardening law & cohesive laws properties.

	R_0 (MPa)	R_∞ (MPa)	k	β	
	400	300	4.4	1	
	E_{coh} (MPa)	Δ_0 (mm)	$\Delta_0 + \Delta_c$ (mm)	D_c	$\bar{\varepsilon}_c^p$
Bi-lin.	10	0.1	1	0.5	–
Lin/plat.	–	0.1	2		0.2

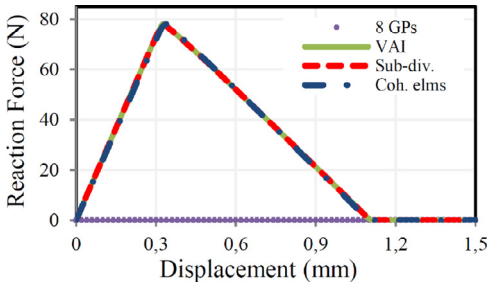

Fig. 6. Single lap test reaction force graph.

where $\underline{\underline{s}}$ is the deviatoric part of the stress tensor and $\underline{\underline{I}}$ the identity tensor. The yield stress σ_Y in (1.17) accounts for isotropic hardening and takes the form of Voce law:

$$\sigma_Y = R_0 + R_\infty[1 - \exp(-k\bar{\varepsilon}^p)]^\beta \tag{1.19}$$

where R_0,R_∞,k, β are material constants describing the isotropic hardening behavior (see Table 1) and $\bar{\varepsilon}^p$ the cumulated plastic strain.

The linear cohesive law used in this part of the study is described in Section 2.2.1 and is similar to the cohesive law governing the behavior of the ABAQUS cohesive elements. The properties of the cohesive law are indicated in Table 1. Since the cohesive crack is inserted in the structure from the very beginning of the analysis, the law is activated within the elements containing the meso–crack from the first time increment.

In the following are conducted four numerical simulations (see Fig. 5 for SL1 and SL2):

- zero-thickness ABAQUS cohesive elements SL.1
- 8-Gauss point standard integration technique SL.2
- sub-division integration technique SL.2
- volume averaging integration (VAI) technique SL.2

SL.1 is used here as a reference solution since ABAQUS cohesive elements are a tool of known accuracy for crack propagation in interfaces.

The numerical results for the four numerical simulations are superimposed in Fig. 6 in terms of reaction force vs. displacement.

According to Fig. 6, the standard Gauss quadrature (8 GPs) is unable to provide a correct prediction of the reaction force (leading to 0 N all along the loading), as expected. On the other hand, the VAI and subdivision schemes give the same response as the cohesive zone model.

4.2. Tensile test – No pre-existing discontinuity

For the tensile test the specimen of Fig. 7 is used. It is discretized using a structured three-dimensional meshing of complete integration hexahedral elements (C3D8 ABAQUS elements) of $0.5 \times 0.5 \times 0.5$ mm^3 (in the area of interest).

The material taken into consideration here is the same as the one of the adherents in Section 4.1, see (1.17-1.19) and Table 1.

The critical value to be attained by an element for localization (activation of XFEM enriched degrees of freedom) is tentatively an arbitrary critical cumulated strain $\bar{\varepsilon}_c^p$, see Table 1, giving the value of $\underline{T}_0$ in (1.8).

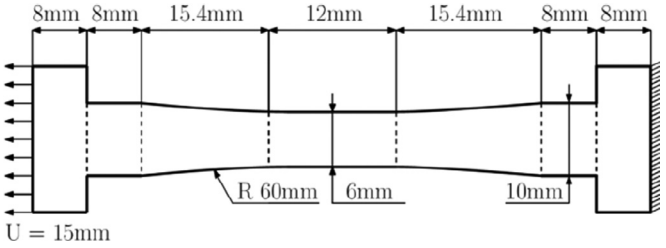

Fig. 7. Traction specimen dimensions.

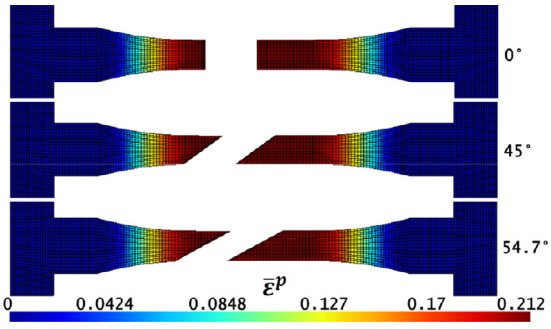

Fig. 8. Tensile specimen cut by 0°, 45° and 54.7° cracks (cumulated plastic strain distribution).

The linear/plateau cohesive law presented in Section 2.2.2 is then used to describe the meso–crack deterioration effect.

In the following are conducted three numerical simulations:

- elasto-plastic response (FEM only)
- sub-division integration technique
- volume averaging integration (VAI) technique

For the last configurations involving the formation and development of a cohesive strong discontinuity, three through-thickness orientations (with respect to the loading direction) of the discontinuity are considered, i.e. 0° (brittle-like fracture), 54.7° (ductile-like fracture [23]) and 45° (worst numerical case). For the 0° case, the crack is forced to appear extremely close to the localized elements' side, ensuring again that one of the created sub-volumes does not contain any integration points. For the two other cases, the crack position within the elements is not imposed since the number of cut elements ensures the existence of multiple sub-volumes that will satisfy the above mentioned extreme condition. The angle of 45° is the most critical numerical case in the sense that, for regular meshing, it guarantees that one out of two elements will not have Gauss points on one side of the crack. The 54.7° case does not necessarily imply the aforementioned problem but it is addressed for physical reasons. The fractured specimens are shown in Fig. 8.

The two integration procedures are detailed below.

- Volume averaging integration (VAI) technique

The localization band propagates throughout the whole width of the specimen (with the chosen angle) when one element attains the critical cumulated strain in one increment. This increment denoted kinc_{LOC} is saved for later use.

- Sub-division integration technique

A band is defined at the very beginning of the analysis with the same path as the one created considering the previous integration technique, resulting in a subdivision in tetrahedra (whose number depends on the way the element is cut into the two sub-volumes) and a distribution of Gauss points from the first increment of the analysis, although the enriched dofs of the localized elements are activated only when the analysis reaches kinc_{LOC}.

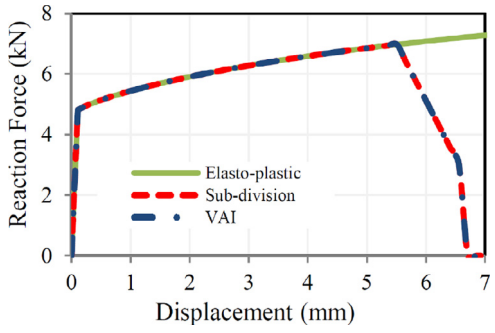

Fig. 9. Tensile specimen reaction force graph (0° case).

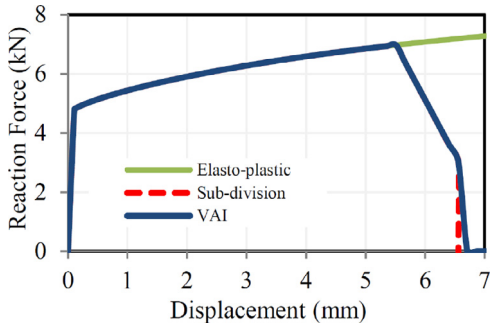

Fig. 10. Tensile specimen reaction force graph (45° case).

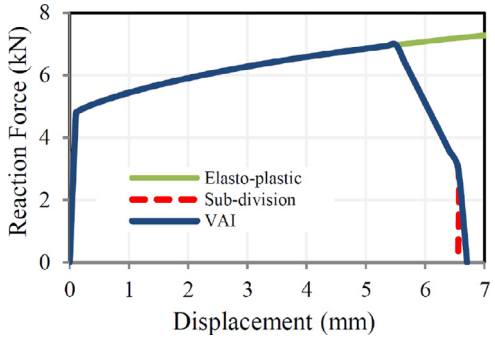

Fig. 11. Tensile specimen reaction force graph (54.7° case).

Indeed, in order to make a successful and pertinent comparison between VAI and the sub-division schemes it is important to control the localization in terms of (i) time of occurrence, (ii) path and (iii) tetrahedra created. It is noted here that in order to calculate the sub-volume values in VAI a triangulation technique is used, dividing the volume into tetrahedra whose volumes can be easily calculated and then summed (these tetrahedra have no other participation in the integration procedure). For both cases, by forcing the band to appear throughout the whole width of the specimen in one increment (kinc_{LOC}) and on the same path, it is possible to control (i), (ii) and (iii) in a way that they are exactly the same for the two schemes. Having isolated these three factors we can compare the schemes solely on their ability to integrate the system of equilibrium equations.

The numerical results for the three numerical simulations are superimposed in Figs. 9, 10 and 11 for the three discontinuity orientations in terms of reaction force vs. displacement. According to Figs. 9, 10 and 11, VAI and subdivision techniques give similar responses. A very slight divergence can be seen in the cases of 45° and 54.7°, but this can be attributed to a difference in the last time step of the analysis.

It should be noted that the standard 8 Gauss point scheme is not presented in any of the two cases because when it was used no analysis was capable to converge after the onset of the localization, so it is omitted.

4.3. Discussion

It is reminded that the subdivision of elements consists in triangulating the sub-volumes $V^+$and V^-, separated by the discontinuity in several tetrahedra and projecting the state variables known at the current integration points onto the newly formed integration points of the tetrahedra. These operations are costly in terms of computation time and potential sources of numerical errors.

The volume averaging integration (VAI) technique does need simply the values of the sub-volumes $V^+$and V^-. The cost in this case is very low and even negligible.

The numerical examples treated in Sections 4.1 and 4.2 have evidenced that both techniques lead to the same results, demonstrating the interest of using the volume averaging integration technique.

It is noteworthy that for tension loading the softening part of the CZM law gives the shape of the overall response in the softening regime. The apparent similarity in the brittle and ductile-like responses in Section 4.2 is due to the fact that the same law was utilized for the sake of simplicity and must not be considered as a generality.

5. Concluding remarks

A volume averaging integration technique or VAI is proposed for the integration of the equilibrium equations when using the XFEM coupled with cohesive zone model. Two different numerical tests, i.e. a single lap joint test and a tensile test, have been realized in order to verify the accuracy of the proposed scheme. It has been shown that the proposed VAI scheme leads to the same level of accuracy as the well-known subdivision technique, while being much simpler to implement and less costly to use.

Acknowledgement

The authors would like to acknowledge the French Direction Générale de l'Armement (DGA) for its support.

Declaration of Competing Interests

None.

References

[1] N. Moës, J. Dolbow, T. Belytschko, A finite element method for crack growth without remeshing, Int. J. Numer. Methods Eng. 46 (1999) 131–150.
[2] G. Wells, L. Sluys, A new method for modelling cohesive cracks using finite elements, Int. J. Numer. Methods Eng. 50 (12) (2001) 2667–2682.
[3] S. Mariani, U. Perego, Extended finite element method for quasi-brittle fracture, Int. J. Numer. Methods Eng. 58 (1) (2003) 103–126.
[4] J. Mediavilla, R. Peerlings, M. Geers, A robust and consistent remeshing-transfer operator for ductile fracture simulations, Comput. Struct. 84 (8–9) (2006) 604–623.
[5] T. Elguedj, A. Gravouil, A. Combescure, Appropriate extended functions for x-fem simulation of plastic fracture mechanics, Comput. Methods Appl. Mech. Eng. 195 (2006) 501–515.
[6] A. Martin, J.B. Esnault, P. Massin, About the use of standard integration schemes for x-fem in solid mechanics plasticity, Comput. Methods Appl. Mech. Eng. 283 (2015) 551–572.
[7] T.J.R. Hughes, Generalization of selective integration procedures to anisotropic and nonlinear media, Int. J. Numer. Methods Eng. 15 (1980) 1413–1418.
[8] T. Belytschko, J. Fish, B.E. Engelman, A finite element with embedded localization zones, Comput. Methods Appl. Mech. 70 (1988) 59–89.
[9] T. Belytschko, T. Black, "Elastic crack growth in finite elements with minimal remeshing, Int. J. Numer. Methods, Eng. 45 (5) (1999) 601–620.

[10] C. Comi, S. Mariani, Extended finite element simulation of quasi-brittle fracture in functionally graded materials, Comput. Methods Appl. Mech. Eng. 196 (41–44) (2007) 4013–4026.
[11] J.P. Crété, P. Longère, J.M. Cadou, Numerical modelling of crack propagation in ductile materials combining the GTN model and X-FEM, Comput. Methods Appl. Mech. Eng. 275 (2014) 204–233.
[12] G. Zi, T. Belytschko, New crack-tip elements for xfem and applications to cohesive cracks, Int. J. Numer. Methods Eng. 57 (2003) 221–2240.
[13] J. Wolf, P. Longère, J.M. Cadou, J.P. Crété, Numerical modeling of strain localization in engineering ductile materials combining cohesive models and X-FEM, Int. J. Mech. Mater. Des. 14 (2017) 177–193.
[14] H. Li, N. Chandra, Analysis of crack growth and crack-tip plasticity in ductile materials using cohesive zone models, Int. J. Plast. 19 (6) (2003) 849–882.
[15] P.P. Camanho and C.G. Davila. Mixed-mode decohesion finite elements for the simulation of delamination in composite materials. NASA/TM-2002-211737, pp. 1–37, 2002.
[16] E. Lorentz, A mixed interface finite element for cohesive zone models, Comput. Methods Appl. Mech. Eng. 198 (2) (2008) 302–317.
[17] G. Alfano, On the influence of the shape of the interface law on the application of cohesive-zone models, Compos. Sci. Technol. 66 (2006) 723–730.
[18] M. Elices, G. Guinea, J. Gomez, The cohesive zone model: advantages, limitations and challenges, Eng. Fract. Mech. 69 (2) (2002) 137–163.
[19] T. Jin, H.M. Mourad, C.A. Bronkhorst, A comparative study of shear band tracking strategies in three-dimensional finite elements with embedded weak discontinuities, Finite Elem. Anal. Des. 155 (2019) 11–31.
[20] J. Shi, D. Chopp, J. Lua, N. Sukumar, T. Belytschko, Abaqus implementation of extended finite element method using a level set representation for three-dimensional fatigue crack growth and life predictions, Eng. Fract. Mech. 77 (14) (2010) 2840–2863.
[21] M.R.R. Seabra, J.M.A. Cesar De Sa, P. Šuštarič, T. Rodič, Some numerical issues on the use of XFEM for ductile fracture, Comput Mech 50 (5) (2012) 611–629.
[22] M.Y. Tsai, J. Morton, An experimental investigation of nonlinear deformations in single-lap joints, Mech. Mater. 20 (3) (1995) 183–194.
[23] A. Pineau, T. Pardoen, 2.06-failure of metals, Compr. Struct. Integr. 2 (2007) 1–202.